remote sensing

MDPI

Article

Cross-Sensor Comparison of SWOT Level-2 Pixel Cloud and ICESat-2 ATL13 Water-Surface Elevations over Tibetan Plateau Lakes

Zhaonan Xue, Lin Liu * and Zhicai Luo

National Gravitation Laboratory and School of Physics, Institute of Geophysics, Huazhong University of Science and Technology, Wuhan 430074, China; xzn19@hust.edu.cn (Z.X.); zcluo@hust.edu.cn (Z.L.)
* Correspondence: liulin616@hust.edu.cn

Highlights

What are the main findings?

- Independent PIXC quality control yielded 89,343 SWOT–ATL13 matches across 50 audit-ready lakes.
- Cross-sensor residuals were scene dependent; lake area was not significantly associated with lake-level RMSE.

What are the implications of the main findings?

- SWOT enables reliable large-scale lake water-level monitoring across the Tibetan Plateau.
- SWOT observations can support multi-satellite fusion and long-term lake-level reconstruction.

Abstract

High-altitude lakes on the Tibetan Plateau (TP) are important components of regional water-cycle regulation and climate responses, yet their long-term monitoring remains challenging due to limited in situ observations and sparse spatial sampling of conventional satellite altimetry. The Surface Water and Ocean Topography (SWOT) mission provides two-dimensional observations of inland water-surface elevation (WSE), offering new opportunities for lake monitoring in remote regions. This study evaluates the applicability of SWOT L2 Pixel Cloud (PIXC) observations for TP lake monitoring through cross-sensor comparison with ICESat-2 ATL13 observations. A total of 50 representative TP lakes were analyzed using quality-controlled SWOT–ICESat-2 matched observations. The results demonstrate that SWOT PIXC and ICESat-2 ATL13 generally capture comparable lake-scale WSE variations across the TP. The mean MAE and RMSE were 0.164 m and 0.231 m, respectively, indicating decimeter-scale cross-sensor consistency for most investigated lakes. Lake area showed no significant association with the RMSE, suggesting that lake size alone does not explain the variability of cross-sensor residuals. Further analysis reveals that residual differences are strongly scene-dependent and reflect combined influences from satellite retrieval characteristics, spatial sampling differences, environmental conditions, and temporal offsets rather than SWOT-only uncertainty. These findings provide an independent assessment of SWOT observations over high-altitude lakes and demonstrate their potential for spatially continuous monitoring of TP lake dynamics. The results also establish a foundation for integrating SWOT with multi-source satellite observations to reconstruct long-term lake water-level and storage variations.

Academic Editor: Andrea Storto

Received: 31 August 2026
Revised: 23 October 2026
Accepted: 26 October 2026
Published: 28 October 2026

Copyright: © 2026 by the authors. Licensee MDPI, Basel, Switzerland. This article is an open access article distributed under the terms and conditions of the Creative Commons Attribution (CC BY) license.

Keywords: the SWOT mission; evaluation; pixel cloud data; Tibetan Plateau; lake water-surface elevation

1. Introduction

The Tibetan Plateau (TP), often referred to as the "Asian Water Tower", contains the world's largest high-altitude lake system, which plays a fundamental role in sustaining the major rivers of Asia and supporting downstream ecosystems and populations [1–3]. As an essential component of the regional hydrological cycle and ecological environment, lakes on the TP regulate surface runoff [4,5], store meltwater and precipitation [6], and modulate regional energy [7] and moisture exchanges [8]. Variations in lake surface elevation are therefore of great scientific interest, as they reflect the combined impacts of climate change, cryospheric melt, and catchment-scale hydrological processes [9,10]. In recent decades, global warming has accelerated the melting of glaciers and permafrost, leading to pronounced expansion or shrinkage of many lakes on the TP [11,12]. Consequently, there is an urgent need to obtain high-precision, long-term, and spatially continuous observations of lake water-surface elevation (WSE) changes on the TP, which are critical for understanding regional water storage variations, hydrological connectivity, and climate–cryosphere–hydrosphere interactions in this sensitive environment.

Previous studies on changes in lake WSE in the TP often relied on in-situ hydrological data [2]. Despite high-frequency availability (e.g., subdaily), in situ measurements of the lake WSE in the TP often suffer from spatial scarcity subject to geographical constraints [13] and are prone to substantial data gaps occurring during freezing periods [14]. These factors reduce their suitability for large-scale hydrological studies. Alternatively, the advancement of radar and laser altimetry satellites [15] provides an opportunity to precisely monitor the lake WSE while greatly expanding the spatial coverage [16]. In practice, it is often necessary to integrate multiple sensors to further extend both the temporal record and the spatial extent of WSE observations. For example, integrated sensors include pulse-limited radar altimeters [17], synthetic aperture radar (SAR) altimeters [18], laser altimeters [19], and optical remote sensing imagery [20]. Despite enhanced performance due to multi-sensor integration, these traditional altimetry missions rely on waveform retracking to derive WSEs from along-track footprints and are fundamentally constrained by orbital coverage [21]. As a result, these limitations reduce the spatial representativeness and continuity of the measurements, particularly for smaller or morphologically complex lakes [22–24]. Improvement of the accuracy and coverage of lake water-level monitoring has become one of the key challenges in current lake hydrological research [25].

To bridge the gap, next-generation satellite altimetry has been proposed and implemented. The Surface Water and Ocean Topography (SWOT) mission, launched in December 2022, was developed within the framework of the Wide Swath Ocean Altimeter (WSOA) program [26]. The satellite is designed to deliver more precise measurements of global surface water and oceans. By employing wide-swath interferometric measurement technology, SWOT is capable of providing two-dimensional observations of both terrestrial water bodies and oceans, thereby addressing some of the key limitations of traditional altimetry, including restricted spatial coverage and long revisit intervals [27]. A central innovation of SWOT is the Ka-band Radar Interferometer (KaRIn), which enables high-resolution, two-dimensional WSE mapping across a swath of 50–60 km [28]. This technological breakthrough marks a shift from point- or track-based measurements to continuous two-dimensional mapping, allowing for almost full coverage of lakes exceeding a certain size threshold. As a result, SWOT significantly enhances both spatial continuity and measurement accuracy relative to traditional satellite altimetry missions.

https://doi.org/10.3390/rs18213713

However, due to the rugged terrain and highly heterogeneous surface conditions of the TP, it is essential to assess the reliability and accuracy of SWOT L2 PIXC observations before applying them to large-scale hydrological studies. In this work, we use the Ice, Cloud, and land Elevation Satellite-2 (ICESat-2) ATL13 product as a benchmark for validation. ICESat-2 provides laser-based photon-counting elevation measurements with centimeter-level precision, and its narrow-beam design enables accurate retrievals of water-surface elevations over inland lakes. These characteristics make ICESat-2 an ideal reference dataset for evaluating the performance of SWOT measurements [29–31]. Although several studies have examined SWOT accuracy over global rivers and selected large lakes [24,32–34], comprehensive evaluations focusing on large lakes (>100 km^2) across the TP are still scarce. Moreover, most existing works have primarily focused on the SWOT L2 LakeSP product, which is derived from L2 PIXC data through additional processing and filtering. As a result, the intrinsic measurement uncertainties and spatial characteristics of the original L2 PIXC data remain less explored, particularly in complex high-altitude environments such as the TP.

In this study, our main focus is the evaluation of SWOT L2 PIXC data for lakes larger than 100 km^2 on the TP, by using the ICESat-2 ATL13 product as the benchmark reference. Through a quantitative comparison of the two satellite datasets, we examine the precision and applicability of SWOT-derived lake WSE on the plateau. The results are expected to provide a robust scientific basis for future applications of multi-satellite data fusion and for advancing regional hydrological studies.

2. Study Area and Data

2.1. Study Area

The TP, often referred to as the "Roof of the World", is the highest and most extensive plateau on Earth, with an average elevation exceeding 4500 m [9]. As a critical regulator of the global climate system, the TP is also known as the "Third Pole" due to its abundant glaciers and snow cover. The unique geomorphological features of the TP have been shaped by a combination of tectonic activity, glacial processes, and erosion, resulting in a complex topography characterized by towering mountains, deep valleys, and widespread lakes [35]. The lakes on the TP are primarily located in enclosed basins, with their surface area fluctuations driven by a balance between precipitation, glacial meltwater, and evaporation [36]. Over 1500 lakes are distributed across the plateau, covering a total area of approximately 50,000 km^2. The TP provides an ideal testing ground for evaluating SWOT performance because it combines large hydrological importance with challenging observation conditions. Its high elevation, complex topography, and large number of lakes make it a representative region for assessing the reliability of SWOT L2 PIXC data in mountainous environments.

This study focuses on lakes larger than 100 km^2 on the TP, as shown in Figure 1, where four lakes are zoomed in for illustration. The lake boundaries were obtained from the shapefiles provided by Zhang [37] and were treated as fixed reference boundaries throughout the analysis. They were used to consistently define the spatial extent of each lake and to constrain the extraction and cross-sensor matching of SWOT PIXC and ICESat-2 ATL13 observations [31]. The adopted boundaries represent reference geometries for data processing rather than time-varying lake shorelines.

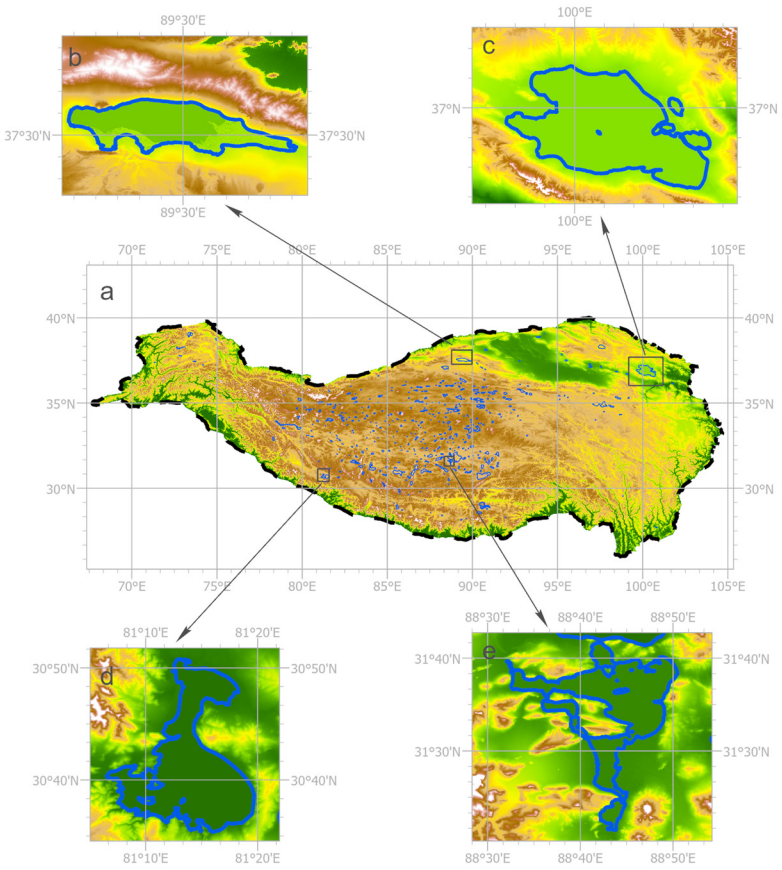


Figure 1. Location of the study area on the Tibetan Plateau (TP): (**a**) overview of the TP and locations of the five study lakes: (**b**) Ayakkum Lake, (**c**) Qinghai Lake, (**d**) Langa Co, and (**e**) Ngoin Co. Blue lines indicate lake boundaries.

2.2. Data

SWOT L2 PIXC data: The SWOT satellite mission primarily provides global measurements of WSEs, including the heights of rivers, lakes, and oceans. Its data products are categorized into multiple levels, including Level 0 (L0), Level 1 (L1), Level 2 (L2), and Level 3 (L3) [38]. L0 and Level 1a (L1a) are considered raw data products, comprising data directly acquired from satellite sensors and data that have undergone basic preprocessing steps, such as denoising and calibration. However, further processing is required to convert these data into scientific products. The SWOT L2 (as summarized in Table 1) terrain data products include a variety of derived topographic data, such as WSEs, riverbed elevation, and lake water-level information. These data, processed through specific algorithms, are well-suited for direct scientific analysis. L3 hydrological data products encompass various derived datasets related to hydrology, such as river discharge, flood extent, and lake water volume changes. These datasets are of significant value for hydrological assessments and water resource management. The SWOT L2 PIXC, a secondary product extracted from SWOT satellite observations, primarily includes elevation information for water bodies. These data are generated by the satellite's primary instrument, the Ka-band Radar Interferometer (KaRIn), which provides high spatial resolution (~10–70 m in the along-track direction and ~50–100 m in the across-track direction) and high vertical accuracy (typically better than 10 cm over water surfaces under nominal conditions) [39]. The processing of SWOT L2 data involves multiple steps of correction and filtering to reduce noise and errors. These processing steps typically include terrain correction, atmospheric corrections (such as adjustments for ionospheric and tropospheric delay effects), and orbit

error adjustments [40]. After these processes, the resulting pixel cloud data contain precise measurements of WSEs.

ICESat-2 data: The ICESat-2 satellite is designed to precisely measure surface elevation changes on Earth, including those of ice sheets, glaciers, forests, and lakes [30]. Its core sensor, the Advanced Topographic Laser Altimeter System (ATLAS), measures surface elevation by emitting high-frequency laser pulses, generating highly accurate digital elevation models. The ATL13 data, classified as a Level 3a product of ICESat-2, is specifically used for measuring the height of inland water bodies. ATL13 provides along-track measurements of WSE, along with standard deviations, subsurface signal (532 nm) attenuation, significant wave height, wind speed, and a rough estimation of underwater topography. These data are available through NASA's Earth data platform (https://search.earthdata.nasa.gov/search (accessed on 15 May 2025)), containing detailed information on geographic location, elevation, and reflectivity. Data processing typically involves temporal and spatial registration, terrain correction, and the separation of signal from noise. The primary reason for selecting ICESat-2 ATL13 data for accuracy assessment is its high precision in measuring inland water body elevations [41]. Additionally, ATL13 data undergo rigorous calibration and validation to ensure data consistency and accuracy. Consequently, ICESat-2 ATL13 data provide a reliable benchmark for evaluating the accuracy of SWOT L2 PIXC data.

Table 1. Summary of SWOT Level 2 High-Resolution (L2_HR) products.

Dataset	Description	Coverage	Format
L2_HR_PIXC/PIXCVec	Pixel cloud data providing geolocated water-surface elevations, backscatter, and corrections; PIXCVec links pixels to hydrologic features.	Pixel cloud (~64 × 64 km²); both swaths	netCDF
L2_HR_RiverSP/RiverAvg	River products defining reaches and nodes with attributes such as elevation, slope, width, and discharge; RiverAvg gives cycle means.	Both swaths/per cycle	shapefiles
L2_HR_LakeSP/LakeAvg	Lake products identifying observed/unobserved lakes with elevation, area, and storage change; LakeAvg gives cycle means.	Both swaths/per cycle	shapefiles
L2_HR_Raster/FPDEM	Gridded data (100–250 m) of elevation, backscatter, and ancillary parameters; FPDEM provides fixed DEMs (~5 m).	Grid (~128 × 128 km²)/geographic tile (~1°)	netCDF

3. Methods

3.1. Processing Chain

In this study, the consistency between SWOT L2 PIXC and ICESat-2 ATL13 WSE observations was assessed following the workflow shown in Figure 2. First, lake boundary data for the TP provided by Zhang were used as fixed spatial references to identify observations located within lake extents. ICESat-2 ATL13 observations falling within these predefined lake boundaries were retained for subsequent cross-sensor comparison. Both ICESat-2 and SWOT datasets underwent consistent preprocessing, including quality control and vertical datum conversion to EGM2008, ensuring that the two datasets were comparable within the same reference framework. For each lake, the nearest available SWOT and ICESat-2 acquisitions were initially paired subject to a maximum absolute temporal separation of 10 days. Sensitivity analyses were subsequently performed using temporal thresholds of 0, 3, 5, and 10 days. Because a temporal offset may contain genuine WSE or

surface-state changes, residuals from non-simultaneous acquisitions were interpreted as cross-sensor differences rather than sensor-specific errors.

To spatially match SWOT observations with ICESat-2 measurements, SWOT PIXC pixels within a 17 m radius of each ATL13 footprint were extracted and averaged to obtain a representative SWOT WSE for each ICESat-2 observation. The 17 m radius was selected based on the approximate diameter of the ICESat-2 laser footprint, providing a physically motivated spatial matching scale for the two datasets. The influence of the buffer radius on the comparison results was further examined using alternative spatial matching distances. The rationale for selecting the 17 m buffer and the corresponding sensitivity analysis is presented in Section 4.2.

Residuals were calculated as the differences between ATL13 elevations and the corresponding SWOT PIXC-derived WSE values, and statistical evaluation was performed using the metrics described in Section 3.2. Two additional sensitivity analyses were conducted to examine the robustness of the results. First, temporal matching thresholds of 0, 3, 5, 7, and 10 days were applied to assess changes in sample coverage and the resulting lake-level RMSE. Second, residual-based removal using 1 × SD, 2 × SD, and 3 × SD criteria were compared with the results obtained without residual-based removal to quantify the influence of residual filtering on the reported RMSE. The results of these sensitivity analyses are presented in Section 4.2.

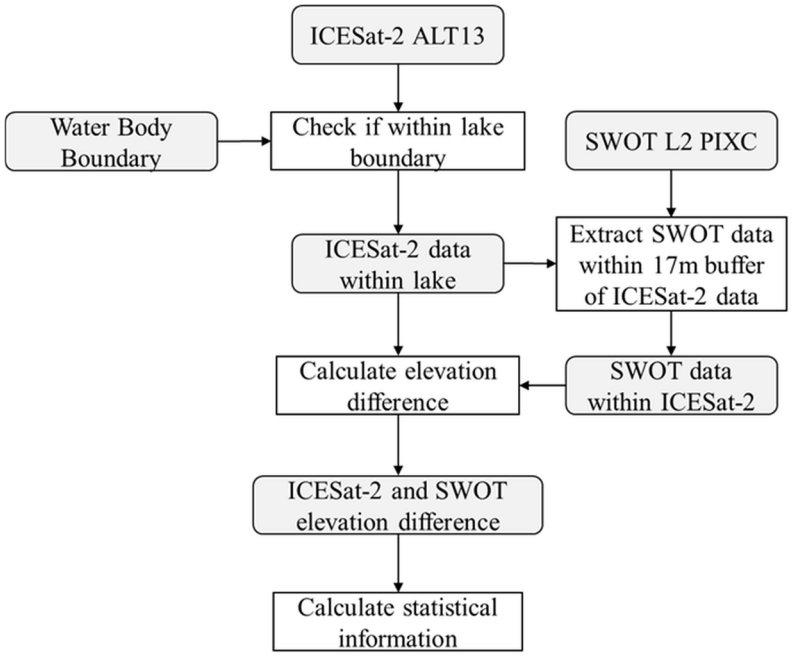


Figure 2. Flowchart of data processing chain for evaluation of SWOT.

3.2. Evaluation Metrics

To comprehensively assess the accuracy of SWOT L2 data compared to ICESat-2 data, we use the following evaluation metrics. Let $d_i = H_{ATL13,i} - H_{SWOT,i}$ for the n finite matched footprints of a lake. We report the mean bias, MAE, RMSE, the sample standard deviation (STD) of d_i about its mean, and Pearson's r between the two matched elevation series. The MAE and RMSE quantify cross-sensor difference magnitude; residual STD describes dispersion after the mean offset; and r describes covariance, not absolute agreement.

Mean Absolute Error (MAE): The MAE measures the average deviation between two datasets, potentially indicating discrepancies arising from temporal mismatches between the observations and from systematic errors. The MAE is defined as:

$$\mathrm{MAE} = \frac{1}{n}\sum_{i=1}^{n}|y_i - \hat{y}_i| \quad (1)$$

where y_i is the observed value from ICESat-2 data for the i-th data point, $\hat{y}_i$ is the corresponding value from SWOT L2 data, and n is the total number of data points.

Root Mean Square Error (RMSE): The RMSE quantifies the overall accuracy of the SWOT L2 PIXC data by measuring the magnitude of the deviations between satellite observations and reference measurements. It reflects the combined effects of random noise and systematic bias, and is particularly sensitive to large errors. The RMSE is defined as:

$$\mathrm{RMSE} = \sqrt{\frac{1}{n}\sum_{i=1}^{n}(y_i - \hat{y}_i)^2} \quad (2)$$

Residual Standard Deviation (STD): The residual STD describes the dispersion of individual residuals (d_i) around the lake-level mean residual, and is used to evaluate the internal variability of cross-sensor WSE differences. It does not represent SWOT-only precision, because the residuals contain combined contributions from SWOT and ICESat-2 measurements, spatial sampling effects, surface state variability, and temporal mismatch. Therefore, the residual STD reflects the consistency of SWOT–ICESat-2 agreement for each lake and is defined as:

$$\mathrm{STD} = \sqrt{\frac{1}{n-1}\sum_{i=1}^{n}\left(d_i - \bar{\mathrm{d}}_i\right)^2} \quad (3)$$

where (d_i) is the elevation difference between SWOT and ICESat-2 for the i-th matched footprint, $(\bar{d})$ is the mean residual for the corresponding lake, and n is the number of finite matched footprints.

Correlation Coefficient (R): The R quantifies the linear relationship between matched ICESat-2 ATL13 and SWOT L2 PIXC elevations. It indicates the degree to which the two datasets exhibit consistent variation patterns but does not evaluate absolute agreement. Therefore, R is interpreted together with bias, the MAE, and RMSE rather than as an independent measure of measurement accuracy. It is defined as:

$$R = \frac{\sum_{i=1}^{n}(y_i - \bar{y})\left(\hat{y}_i - \bar{\hat{y}}\right)}{\sqrt{\sum_{i=1}^{n}(y_i - \bar{y})^2 \sum_{i=1}^{n}\left(\hat{y}_i - \bar{\hat{y}}\right)^2}} \quad (4)$$

where $\bar{y}$ is the mean of the ICESat-2 data and $\bar{\hat{y}}$ is the mean of the SWOT data.

These evaluation metrics collectively characterize the agreement and consistency between SWOT L2 PIXC and ICESat-2 ATL13 WSE observations. The MAE and RMSE quantify the magnitude of cross-sensor elevation differences, the STD describes the variability of residuals around the lake-level mean residual, and R evaluates the linear covariation between the two datasets. Together, these metrics provide a comprehensive assessment of SWOT PIXC performance for lake-level monitoring over the Tibetan Plateau, while the derived residual statistics should be interpreted as cross-sensor differences that incorporate contributions from both datasets, spatial sampling, environmental conditions, and temporal mismatch rather than as estimates of SWOT-only absolute accuracy.

4. Results

4.1. Overall Assessment

Table 2 summarizes the statistical characteristics of the cross-sensor comparison for the 50 retained lakes, including lake area, the MAE, residual STD, RMSE, R, bias, and N, where N represents the number of finite footprint–neighborhood matched pairs. Across all retained lakes, the mean (median) MAE was 0.164 (0.145) m, while the mean (median) RMSE was 0.231 (0.186) m, indicating generally consistent agreement between SWOT PIXC and ICESat-2 ATL13 WSE observations across the Tibetan Plateau lakes. Eight lakes exhibited RMSE values greater than 0.3 m, suggesting larger cross-sensor residual variability in these cases and motivating further investigation of potential environmental and observational factors. Four representative lakes were selected for detailed analysis to further examine the spatial and temporal characteristics of SWOT–ICESat-2 residuals.

Table 2. The fundamental statistical metrics for 50 typical lakes.

Lake Name	Area/km²	N	Bias/m	MAE/m	Residual STD/m	RMSE/m
Qinghai Lake	4348.252	2269	−0.061	0.148	0.175	0.185
Selin Co	2300.370	2368	0.011	0.242	0.307	0.308
Nam Co	2024.214	2701	−0.086	0.139	0.150	0.173
Zhari Namco	1000.572	3570	−0.045	0.105	0.126	0.134
Ayakkum Lake	986.901	3072	0.018	0.149	0.185	0.186
Bangong Co	671.195	386	0.014	0.106	0.135	0.136
Wulanwula Lake	650.997	753	−0.065	0.127	0.147	0.160
Ngoring Lake	642.070	1489	−0.050	0.098	0.161	0.169
Har Lake	609.044	471	−0.239	0.513	0.599	0.644
Chibzhang Co	541.178	5068	−0.006	0.141	0.179	0.179
Aqqikkol Lake	538.454	1312	−0.095	0.174	0.198	0.220
Gyaring Lake	524.795	1173	−0.038	0.110	0.133	0.138
Dogai Coring	492.405	1615	−0.015	0.115	0.145	0.146
Taro Co	484.650	333	0.010	0.140	0.184	0.184
Ngangze Co	471.605	3543	−0.020	0.156	0.197	0.198
Xijir Ulan Lake	462.689	509	0.005	0.089	0.114	0.114
Mapam Yumco	412.695	81	0.038	0.112	0.132	0.136
Lumajiangdong Co	384.674	3833	−0.114	0.181	0.196	0.227
Urru Co	356.569	459	−0.003	0.095	0.127	0.127
Hoh Xil Lake	350.376	7180	−0.116	0.194	0.215	0.244
Jingyu Lake	339.574	757	−0.097	0.135	0.135	0.166
Dagze Co	311.037	667	−0.008	0.140	0.178	0.178
Puma Yumco	290.428	206	−0.034	0.211	0.256	0.257
Lexiewudan Co	273.299	631	−0.006	0.108	0.135	0.135
Paiku Co	272.952	541	−0.015	0.117	0.146	0.146
Co Ngoin1	268.419	1260	−0.157	0.268	0.335	0.370
Ake Sayi Lake	258.259	2959	−0.007	0.201	0.252	0.252
Langa Co	256.242	3659	−0.081	0.193	0.228	0.242
Bamco	255.285	2173	−0.022	0.119	1.284	1.284
Gozha Co	245.342	833	−0.125	0.313	0.377	0.397
Zige Tangco	238.307	1952	−0.075	0.174	0.203	0.216
Co Nyi	166.908	380	−0.062	0.100	0.110	0.126
Memar Co	166.673	756	−0.057	0.117	0.138	0.150
Yaggain Co1	158.752	628	−0.077	0.107	0.107	0.131
Margai Caka	158.052	389	0.043	0.099	0.119	0.127

Dung Co	151.442	10,030	−0.219	0.237	0.178	0.282
Monco Bunnyi	150.782	892	−0.043	0.148	0.184	0.189
Palung Co	144.645	1231	0.106	0.156	0.169	0.199
Bong Co	143.978	2797	0.056	0.336	0.427	0.430
Bangdag Co	142.919	1993	−0.098	0.149	0.162	0.189
Tso moriri	142.538	5137	−0.165	0.266	0.302	0.344
Mingjing Lake	124.259	178	−0.065	0.096	0.103	0.122
Bangkog Co	123.872	359	−0.084	0.105	0.094	0.126
Chem Co	121.531	1363	−0.060	0.161	0.216	0.224
Xiangyang Lake	121.006	1048	−0.071	0.100	0.106	0.127
Dawa Co	118.202	518	0.002	0.156	0.196	0.196
Amu Co	114.980	154	0.020	0.085	0.107	0.108
Sugan Lake	107.541	871	−0.228	0.341	0.368	0.432
Dong Co	105.428	1739	0.032	0.152	0.192	0.194
Ma'erxia Co	102.070	1057	−0.067	0.154	0.184	0.196

To investigate whether lake size is associated with cross-sensor residual variability, lake-level RMSE values were compared with lake area using Pearson correlation on $\log_{10}$-transformed area and Spearman rank correlation. These analyses considered one RMSE value per lake and were used only to evaluate statistical associations rather than to infer causal relationships.

Figure 3 illustrates the distribution of lake-level RMSE values across lakes with different sizes. Although RMSE values show substantial variability among individual lakes, no clear size-dependent pattern is observed. The Pearson correlation between the $\log_{10}$(area) and the RMSE was −0.03 (p = 0.822), while the Spearman rank correlation was −0.06 (p = 0.668), indicating a negligible statistical relationship between lake area and cross-sensor residual magnitude. Several lakes exhibited relatively larger RMSE values; however, these cases occurred across different lake-size ranges rather than being concentrated within a specific area category. Overall, the results suggest that SWOT–ICESat-2 agreement varies among lakes and does not exhibit an evident dependence on lake size within the investigated dataset.

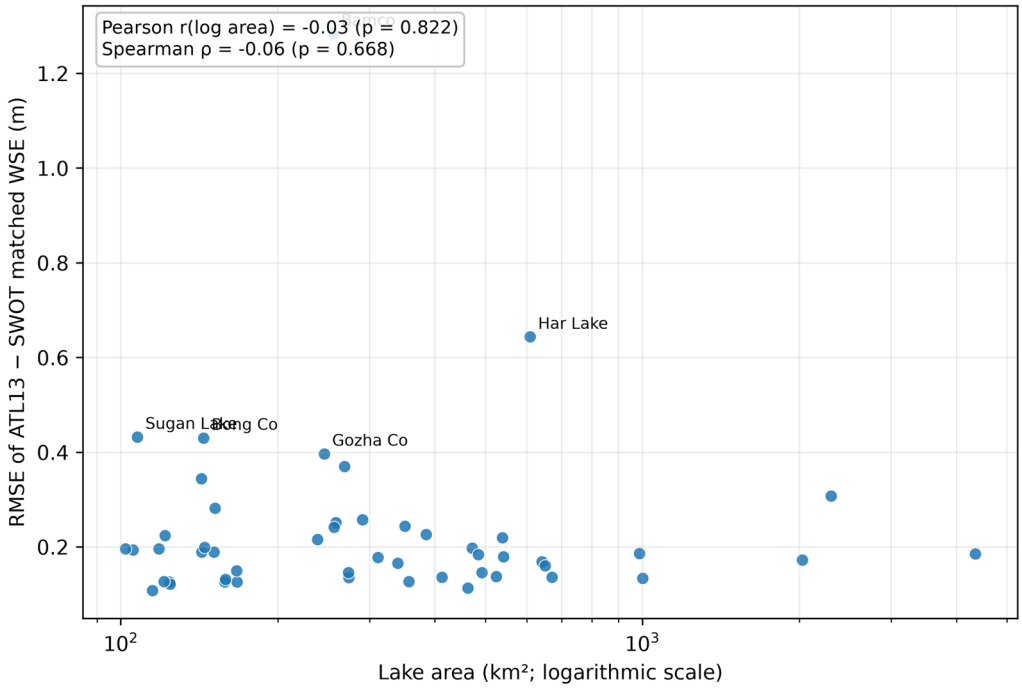


Figure 3. Relationship between the lake area (log-transformed) and the RMSE of WSE matches.

4.2. Sensitivity to Matching Criteria and Residual Filtering

The sensitivity analyses examined the effects of spatial matching, shoreline exclusion, temporal separation, and residual filtering on the cross-sensor comparison results. The mean lake-level RMSE was 0.229, 0.231, 0.199, and 0.160 m for matching radii of 10, 17, 25, and 50 m, respectively. The decrease in the RMSE with increasing neighborhood size indicates that spatial averaging influences the magnitude of cross-sensor residuals. Larger neighborhoods also broaden the spatial support of the SWOT estimates and increase the potential for pixel reuse and overlap between neighboring matching areas. The similar RMSE values obtained with 10 and 17 m radii indicate relatively stable results at smaller matching scales. Accordingly, the 17 m radius was selected based on the approximate diameter of the ICESat-2 laser footprint, providing a physically motivated local matching scale while limiting excessive spatial averaging. At this radius, increasing the shoreline exclusion distance from 0 to 250 m changed the mean RMSE from 0.231 to 0.230 m and reduced the number of matched pairs from 89,343 to 85,144. This small change indicates that shoreline exclusion had a limited influence on the regional mean RMSE under the adopted boundary and quality-control criteria.

Temporal matching sensitivity was assessed by examining the trade-off between temporal coincidence and sample coverage (Figure 4). Same-UTC-date comparisons were available for only two lakes, yielding 3828 matched observations. When the maximum temporal separation was increased to 3, 5, 7, and 10 days, the number of retained lakes increased to 24, 37, 43, and 45, respectively, with 34,861, 59,195, 72,899, and 73,945 matched observations. The complete nearest-acquisition dataset comprised 50 lakes and 89,343 matched observations. These results demonstrate that relaxing the temporal matching criterion substantially increased sample coverage across the Tibetan Plateau. The mean lake-level RMSE did not increase monotonically with the temporal window, indicating that differences among the temporal subsets were also influenced by changes in lake and scene composition. In addition, the same-date subset contained only two lakes, limiting the representativeness of its RMSE for the regional sample.

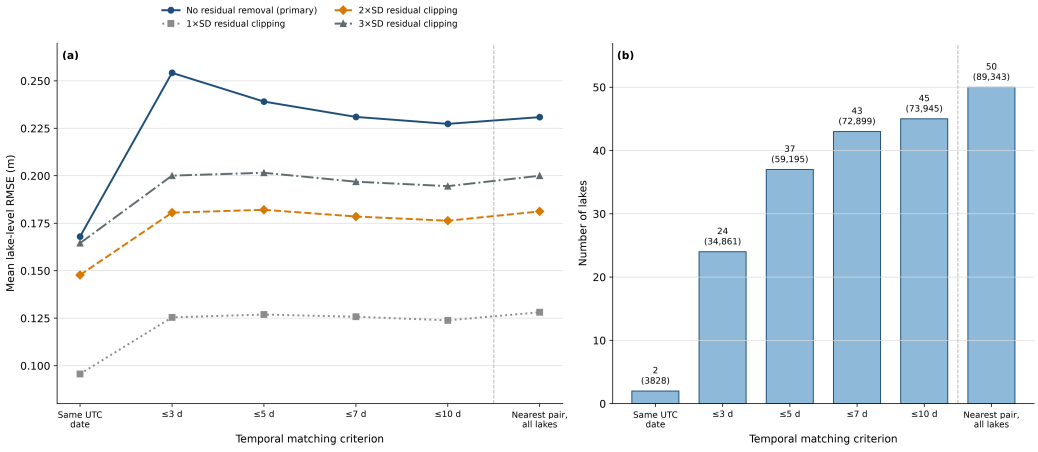


Figure 4. Sensitivity of the cross-sensor RMSE to temporal matching and residual filtering. (**a**) Mean lake-level RMSE under different temporal matching criteria and residual-filtering thresholds. (**b**) Retained lakes and matched observations under each temporal criterion. Lake counts are shown above the bars, with matched-observation counts in parentheses.

Residual-filtering sensitivity was evaluated by comparing results obtained without residual-based removal with those obtained using 1 × STD, 2 × STD, and 3 × STD thresholds (Figure 4). Without residual filtering, all 89,343 matched observations were retained, and the mean lake-level RMSE was 0.231 m. Applying the 1 × STD, 2 × STD, and 3 × STD criteria retained 63,456 (71.0%), 85,363 (95.5%), and 88,872 (99.5%) observations,

respectively, with corresponding mean lake-level RMSE values of 0.128, 0.181, and 0.200 m. The progressively lower RMSE values under stricter filtering criteria demonstrate the influence of residual exclusion on the reported cross-sensor differences. In particular, the 2 × STD criterion reduced the mean RMSE by approximately 22% relative to the unfiltered result while retaining 95.5% of the matched observations.

4.3. Regional Analysis

Four lakes were selected as representative examples to illustrate the characteristics of SWOT–ICESat-2 residuals under different observation conditions. The case studies focus on the spatial distribution of observations, matched elevation variations, residual characteristics, and along-latitude elevation patterns. The observed differences between SWOT PIXC and ICESat-2 ATL13 represent combined effects from both satellite products, including differences in data processing, spatial sampling, surface observation conditions, and temporal mismatch. Therefore, these examples are used to describe residual patterns rather than to attribute the observed differences to a single data source. ICESat-2 ATL13 observations are used as an independent satellite reference for cross-comparison to evaluate the capability of SWOT PIXC in capturing lake water-level variations over the Tibetan Plateau.

The Ayakkum Lake was observed by both sensors on 20 October 2023 (Figure 5). After quality control, 3072 matched footprints were retained. The bias, MAE, residual STD, RMSE, and Pearson correlation coefficient were 0.018 m, 0.149 m, 0.185 m, 0.186 m, and 0.384, respectively. Figure 5a shows the spatial distribution of the quality-controlled SWOT PIXC observations and ICESat-2 ATL13 locations. The two datasets exhibit a consistent spatial coverage pattern over the lake surface, providing comparable observations for cross-sensor evaluation. Figure 5b presents the matched WSE observations from both datasets. The overall elevation variations observed by SWOT PIXC and ICESat-2 ATL13 are similar, indicating that both datasets capture the general spatial characteristics of the lake water surface. Meanwhile, differences between individual matched observations are evident, with SWOT-derived elevations showing larger local fluctuations compared with the ATL13 elevation sequence.

The residual distribution (Figure 5c) shows that the elevation differences are mainly concentrated around the mean residual, with most values distributed within approximately ±0.3 m. The small bias (0.018 m) indicates that no obvious overall elevation offset exists between the two datasets for this observation period. However, the residual dispersion reflected by the STD and RMSE demonstrates that differences remain at the footprint scale. These differences may arise from multiple sources, including the retrieval characteristics of the two satellite products, differences in observation scales, and short-term variations in lake surface conditions.

The along-latitude profiles (Figure 5d) show that both datasets capture a similar large-scale elevation trend across Ayakkum Lake. The ATL13 profile presents relatively smooth variations, whereas the SWOT-derived profile contains more local fluctuations. This difference reflects the distinct observation and processing characteristics of the two satellite products. The moderate correlation coefficient (R = 0.384) suggests that the point-level variations between the two datasets are not completely consistent, and therefore the correlation coefficient should be interpreted together with residual magnitude metrics rather than as an independent indicator of agreement. Overall, Ayakkum Lake represents a case where SWOT PIXC and ICESat-2 ATL13 show comparable lake-scale elevation patterns, while footprint-level differences remain due to the combined effects of satellite observation and data processing characteristics.

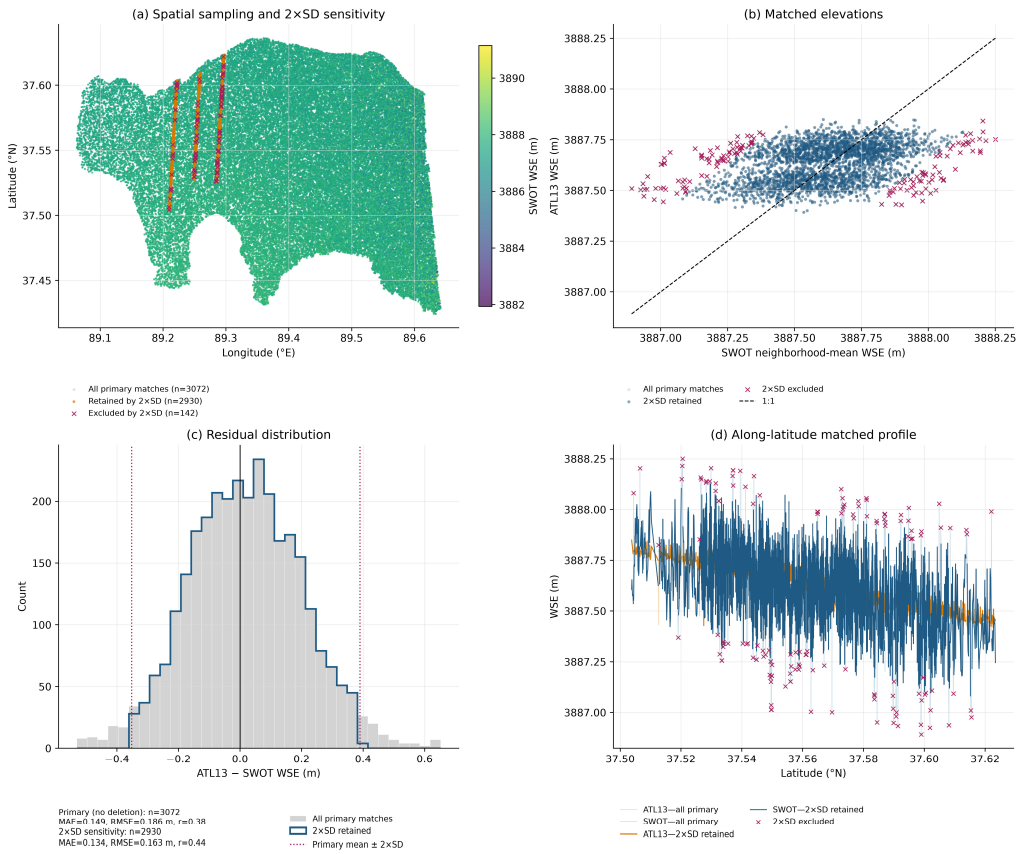


Figure 5. Ayakkum Lake: (**a**) quality-controlled SWOT PIXC and ICESat-2 ATL13 observation locations; (**b**) matched WSEs from SWOT PIXC and ATL13; (**c**) ATL13–SWOT residuals; and (**d**) along-latitude profiles of the matched elevations.

To assess cross-sensor consistency over a very large lake with broad spatial coverage, Qinghai Lake was selected as a representative case. ICESat-2 ATL13 observations acquired on 22 October 2023 and SWOT PIXC observations acquired on 26 October 2023 were compared (Figure 6). After quality control, 2269 matched footprints were retained, with bias, MAE, residual STD, RMSE, and Pearson correlation coefficient values of −0.061 m, 0.148 m, 0.175 m, 0.185 m, and 0.239, respectively. Both datasets capture similar overall water-surface elevation variations across Qinghai Lake, consistent with the pattern observed for Ayakkum Lake. However, greater local dispersion can be observed in some SWOT-derived elevations, particularly near lake boundaries (Figure 6a). This difference may result from the combined effects of observation geometry, spatial sampling differences, and surface conditions, rather than a single controlling factor. Overall, the Qinghai Lake case demonstrates that SWOT PIXC and ICESat-2 ATL13 can capture comparable large-scale lake-level patterns, while footprint-scale residual variability remains present in cross-sensor comparisons.

For Langa Co, SWOT PIXC observations acquired on 24 October 2023 were compared with ICESat-2 ATL13 observations acquired on 27 October 2023 (Figure 7). A total of 3659 matched footprints were retained after quality control, with bias, MAE, residual STD, RMSE, and Pearson correlation coefficient values of −0.081 m, 0.193 m, 0.228 m, 0.242 m, and 0.096, respectively. Compared with the previous cases, Langa Co exhibits larger residual variability and weaker pointwise correlation between the two datasets. Figure 7a shows that relatively large deviations are mainly concentrated in several lake-margin regions, suggesting that local observation conditions may influence the cross-sensor differences. These deviations may involve multiple factors, including observation geometry, spatial sampling differences, shoreline-related mixed observations, and short-term

surface changes, and cannot be attributed to a single factor. Overall, Langa Co represents a case where local residual variations are more pronounced, while the cross-sensor differences should be interpreted as the combined outcome of both satellite observations and observation conditions.

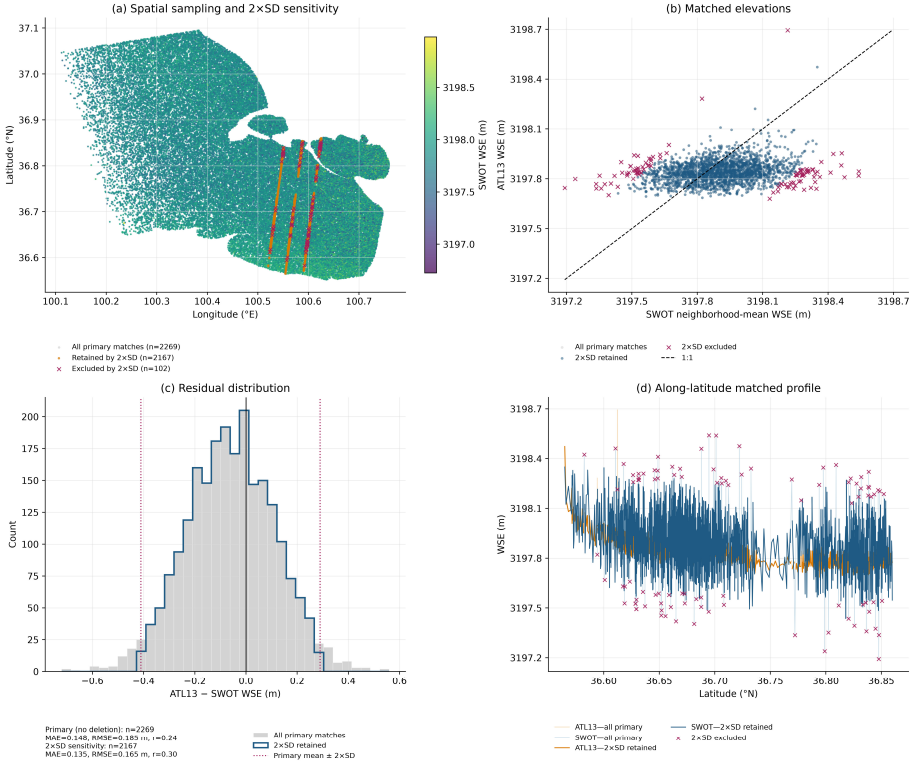


Figure 6. Qinghai Lake: (**a**) quality-controlled SWOT PIXC and ICESat-2 ATL13 observation locations; (**b**) matched WSEs from SWOT PIXC and ATL13; (**c**) ATL13–SWOT residuals; and (**d**) along-latitude profiles of the matched elevations.

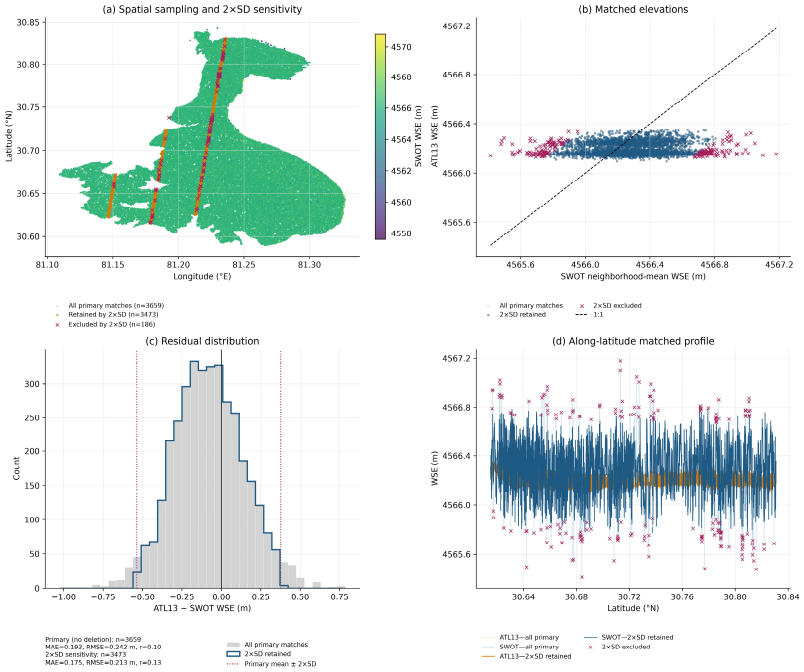


Figure 7. Langa Co: (**a**) quality-controlled SWOT PIXC and ICESat-2 ATL13 observation locations; (**b**) matched WSEs from SWOT PIXC and ATL13; (**c**) ATL13–SWOT residuals; and (**d**) along-latitude profiles of the matched elevations.

The Ngoin Co observations were acquired eight days apart, on 10 and 18 November 2023 (Figure 8), during the period approaching seasonal freeze-up. After quality control, 1260 matched footprints were retained. The bias, MAE, residual STD, RMSE, and Pearson correlation coefficient values were −0.157 m, 0.268 m, 0.335 m, 0.370 m, and 0.088, respectively. Compared with the other case lakes, Ngoin Co exhibited larger residual variability and weaker pointwise correlation between SWOT PIXC and ICESat-2 ATL13 observations.

The eight-day separation means that the observed residuals combine differences between the two satellite products and their processing approaches with any genuine WSE or surface-state changes occurring between acquisitions. The timing of the observations, close to seasonal freeze-up, provides relevant environmental context for interpreting this case. However, in the absence of contemporaneous ice, meteorological, or in situ observations, the contributions of these factors cannot be separated. Ngoin Co therefore represents a case of relatively large cross-sensor differences under non-simultaneous observation conditions, highlighting the importance of considering temporal separation and surface conditions when interpreting satellite-based lake WSE comparisons.

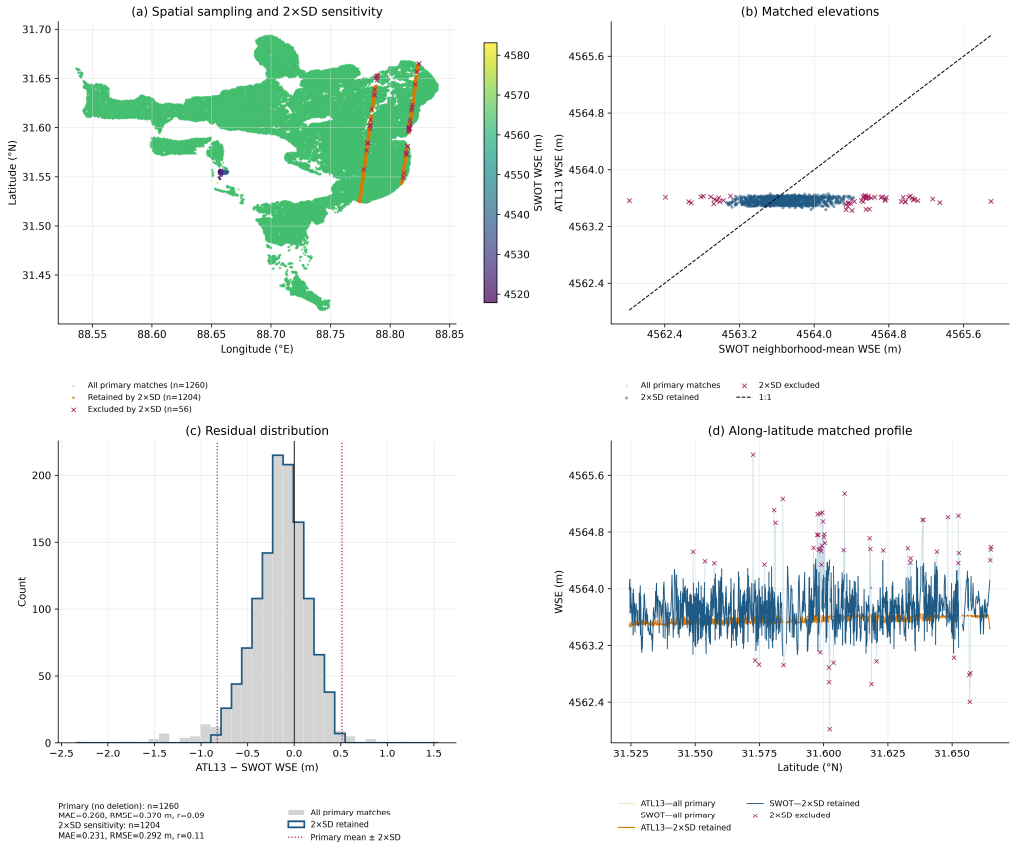


Figure 8. Ngoin Co: (**a**) quality-controlled SWOT PIXC and ICESat-2 ATL13 observation locations; (**b**) matched WSEs from SWOT PIXC and ATL13; (**c**) ATL13–SWOT residuals; and (**d**) along-latitude profiles of the matched elevations.

5. Discussion

The evaluation demonstrates that SWOT L2 PIXC provides decimeter-scale consistency with ICESat-2 ATL13 observations for most Tibetan Plateau lakes. However, the derived residuals represent cross-sensor differences rather than SWOT-only errors, because they include contributions from both satellite products, spatial sampling differences, surface conditions, geophysical corrections, and temporal offsets. Across the 50 retained lakes, the mean and median RMSE were 0.231 m and 0.186 m, respectively, while the mean and median MAE were 0.164 m and 0.145 m. The difference between mean and

median values reflects the influence of several high-residual cases, such as Bamco (RMSE = 1.284 m), and highlights the heterogeneous observation conditions across the Tibetan Plateau. Therefore, the MAE, RMSE, bias, residual STD, and correlation coefficient should be interpreted jointly rather than as independent indicators of SWOT accuracy.

A major advantage of SWOT is its two-dimensional observation capability, which provides spatially continuous water-surface elevation information across entire lake extents and complements the sparse sampling of traditional altimetry and laser altimetry missions. The comparison with ICESat-2 shows that SWOT and ATL13 generally capture consistent lake-scale elevation patterns, although pointwise correlations may remain low for lakes with limited internal WSE variability. The case studies further demonstrate that residual characteristics vary among different scenes. Lakes with different observation conditions, such as large water bodies, complex surrounding terrain, or transitional surface states, may exhibit increased residual variability. These differences likely reflect the combined influence of observation geometry, spatial-support differences, retrieval characteristics, and temporal changes between acquisitions, rather than a single dominant error source. The spatial sensitivity analysis also indicates that residual magnitude depends on the matching scale, emphasizing the importance of considering spatial consistency when comparing satellite-derived lake elevations.

Several limitations should be considered. First, no available in situ observations were incorporated because the existing measurements did not simultaneously satisfy the temporal coincidence and spatial representativeness requirements for the selected satellite scenes. Measurements with large temporal gaps may mix actual lake-level changes with sensor differences, while stations located away from satellite footprints may introduce spatial-support mismatch. Therefore, the lack of suitable field observations is a limitation of the current assessment rather than evidence that in situ validation is unnecessary. Second, the residuals combine uncertainties from both SWOT and ICESat-2, and the current analysis cannot fully separate instrument, processing, and environmental contributions. In addition, overlapping spatial matching neighborhoods may reduce the statistical independence of individual comparisons, and longer SWOT records are required for robust long-term trend analysis.

Future studies should integrate SWOT with historical altimetry, ICESat-2, optical remote sensing, GRACE/GRACE-FO, climate reanalysis, and hydrological models to construct long-term and spatially continuous lake-change datasets. SWOT is particularly valuable as a spatial constraint for extending lake-level monitoring beyond sparse satellite tracks and improving the reconstruction of lake storage variations before and after the SWOT era. With longer observation records and improved processing strategies, SWOT–multi-source data integration will provide new opportunities for investigating Tibetan Plateau lake dynamics and their responses to climate and cryospheric changes.

6. Conclusions

This study conducted a cross-sensor evaluation of SWOT L2 PIXC water-surface elevation observations over Tibetan Plateau lakes using ICESat-2 ATL13 as an independent satellite reference. A total of 50 lakes and 89,343 matched SWOT–ICESat-2 footprints were retained after consistent preprocessing and quality control. The results demonstrate that SWOT PIXC can capture lake-scale water-surface elevation variations across the Tibetan Plateau, while the observed differences between SWOT and ICESat-2 represent combined effects from satellite observations, spatial sampling differences, environmental conditions, and temporal offsets rather than SWOT-only errors.

The statistical evaluation shows that the mean (median) MAE and RMSE were 0.164 (0.145) m and 0.231 (0.186) m, respectively, indicating generally decimeter-scale agreement between SWOT PIXC and ICESat-2 ATL13 for most investigated lakes. Lake area

showed no significant relationship with the RMSE, suggesting that lake size alone does not determine the magnitude of cross-sensor residual variability. Sensitivity analysis further demonstrated that the derived residuals depend on the spatial matching scale, while changes in shoreline exclusion distance had limited influence on the regional-scale results under the adopted evaluation framework.

The analysis of four representative lakes revealed distinct scene-dependent residual characteristics. Ayakkum Lake and Qinghai Lake showed consistent lake-scale elevation patterns between SWOT and ICESat-2, while Langa Co and Ngoin Co exhibited larger residual variability under more complex observation conditions. These cases highlight that differences between satellite-derived water levels are influenced by multiple factors, including observation timing, spatial sampling characteristics, and changing surface conditions, and should not be attributed to a single data source or error mechanism.

Although suitable in situ measurements were unavailable for direct validation due to limitations in temporal coincidence and spatial representativeness, the cross-sensor framework developed in this study provides an independent assessment of SWOT applicability for high-altitude lake monitoring. Future integration of SWOT with ICESat-2, historical altimetry missions, optical remote sensing, gravimetry, and hydrological models will provide new opportunities to construct long-term, spatially continuous lake water-level and storage datasets over the Tibetan Plateau.

Overall, this study demonstrates the capability of SWOT L2 PIXC to provide valuable two-dimensional observations of Tibetan Plateau lakes water surfaces, and establishes a foundation for multi-source satellite fusion and long-term lake change monitoring in high-altitude regions.

Author Contributions: Conceptualization, L.L. and Z.X.; methodology, Z.X.; software, Z.X.; validation, Z.L., L.L. and Z.X.; investigation, Z.X.; resources, Z.X.; data curation, Z.X.; writing—original draft preparation, Z.X.; writing—review and editing, Z.L. and L.L.; visualization, Z.X.; supervision, Z.L.; funding acquisition, L.L. All authors have read and agreed to the published version of the manuscript.

Funding: This work was supported by the CRSRI Open Research Program (CKWV2025958/KY) and the National Natural Science Foundation of China (42274028, 42274112).

Data Availability Statement: SWOT L2_HR_PIXC data are publicly available through NASA Earthdata and PO.DAAC. Exact SWOT granule names, PGE/product versions, and acquisition times are listed in SWOT_granule_manifest.csv. ICESat-2 ATL13 version 007 is available through NASA Earthdata/NSIDC (product DOI: 10.5067/ATLAS/ATL13.007). Public access information for the SWOT and ICESat-2 ATL13 products has been specified, and the archived dataset/code information is provided through Zenodo DOI 10.5281/zenodo.23076827.

Acknowledgments: During the preparation of this manuscript, the authors used ChatGPT 6.0 (OpenAI) for the purposes of language editing and improving the clarity and readability of the manuscript. The authors have reviewed and edited the output and take full responsibility for the content of this publication.

Conflicts of Interest: The authors declare no conflicts of interest.

References

1. Immerzeel, W.W.; Lutz, A.F.; Andrade, M.; Bahl, A.; Biemans, H.; Bolch, T.; Hyde, S.; Brumby, S.; Davies, B.J.; Elmore, A.C.; et al. Importance and Vulnerability of the World's Water Towers. *Nature* **2020**, *577*, 364–369. https://doi.org/10.1038/s41586-019-1822-y.
2. Yao, T.; Bolch, T.; Chen, D.; Gao, J.; Immerzeel, W.; Piao, S.; Su, F.; Thompson, L.; Wada, Y.; Wang, L.; et al. The Imbalance of the Asian Water Tower. *Nat. Rev. Earth Environ.* **2022**, *3*, 618–632. https://doi.org/10.1038/s43017-022-00299-4.
3. Miao, C.; Immerzeel, W.W.; Xu, B.; Yang, K.; Duan, Q.; Li, X. Understanding the Asian Water Tower Requires a Redesigned Precipitation Observation Strategy. *Proc. Natl. Acad. Sci. USA* **2024**, *121*, e2403557121. https://doi.org/10.1073/pnas.2403557121.
4. Wang, Y.; Ye, A.; Zhang, Y.; Yang, F. The Quantitative Attribution of Climate Change to Runoff Increase over the Qinghai-Tibetan Plateau. *Sci. Total Environ.* **2023**, *897*, 165326. https://doi.org/10.1016/j.scitotenv.2023.165326.
5. Fan, X.; Wang, L.; Liu, H.; Chen, D.; Song, L.; Wang, Y.; Qi, J.; Chai, C.; Liu, R.; Li, X.; et al. Tibetan Plateau Runoff and Evapotranspiration Dataset by an Observation-Constrained Cryosphere-Hydrology Model. *Sci. Data* **2024**, *11*, 773. https://doi.org/10.1038/s41597-024-03623-3.
6. Zou, Y.; Kuang, X.; Feng, Y.; Jiao, J.J.; Liu, J.; Wang, C.; Fan, L.; Wang, Q.; Chen, J.; Ji, F.; et al. Solid Water Melt Dominates the Increase of Total Groundwater Storage in the Tibetan Plateau. *Geophys. Res. Lett.* **2022**, *49*, e2022GL100092. https://doi.org/10.1029/2022GL100092.
7. Tang, W.; Xu, S.; Zhou, X.; Yang, K.; Wang, Y.; Qin, J.; Wang, H.; Li, X. Meeting China's Electricity Demand with Renewable Energy over Tibetan Plateau. *Sci. Bull.* **2023**, *68*, 39–42. https://doi.org/10.1016/j.scib.2022.12.012.
8. Huang, J.; Zhou, X.; Wu, G.; Xu, X.; Zhao, Q.; Liu, Y.; Duan, A.; Xie, Y.; Ma, Y.; Zhao, P.; et al. Global Climate Impacts of Land-Surface and Atmospheric Processes over the Tibetan Plateau. *Rev. Geophys.* **2023**, *61*, e2022RG000771. https://doi.org/10.1029/2022RG000771.
9. Immerzeel, W.W.; van Beek, L.P.H.; Bierkens, M.F.P. Climate Change Will Affect the Asian Water Towers. *Science* **2010**, *328*, 1382–1385. https://doi.org/10.1126/science.1183188.
10. Jiang, L.; Nielsen, K.; Andersen, O.B. Improvements in Mountain Lake Monitoring from Satellite Altimetry over the Past 30 Years–Lessons Learned from Tibetan Lakes. *Remote Sens. Environ.* **2023**, *295*, 113702. https://doi.org/10.1016/j.rse.2023.113702.
11. Kang, S.; Xu, Y.; You, Q.; Flugel, W.-A.; Pepin, N.; Yao, T. Review of Climate and Cryospheric Change in the Tibetan Plateau. *Env. Res. Lett.* **2010**, 9, 015101.
12. Ye, Q.; Zong, J.; Tian, L.; Cogley, J.G.; Song, C.; Guo, W. Glacier Changes on the Tibetan Plateau Derived from Landsat Imagery: Mid-1970s–2000–13. *J. Glaciol.* **2017**, *63*, 273–287. https://doi.org/10.1017/jog.2016.137.
13. Yang, S.; Wang, P.; Lou, H.; Wang, J.; Zhao, C.; Gong, T. Estimating River Discharges in Ungauged Catchments Using the Slope–Area Method and Unmanned Aerial Vehicle. *Water* **2019**, *11*, 2361. https://doi.org/10.3390/w11112361.
14. Lei, Y.; Yao, T.; Yang, K.; Sheng, Y.; Kleinherenbrink, M.; Yi, S.; Bird, B.W.; Zhang, X.; Zhu, L.; Zhang, G. Lake Seasonality across the Tibetan Plateau and Their Varying Relationship with Regional Mass Changes and Local Hydrology. *Geophys. Res. Lett.* **2017**, *44*, 892–900. https://doi.org/10.1002/2016GL072062.
15. Crétaux, J.-F.; Birkett, C. Lake Studies from Satellite Radar Altimetry. *Comptes Rendus Géosci.* **2006**, *338*, 1098–1112. https://doi.org/10.1016/j.crte.2006.08.002.
16. Li, X.; Long, D.; Huang, Q.; Han, P.; Zhao, F.; Wada, Y. High-Temporal-Resolution Water Level and Storage Change Data Sets for Lakes on the Tibetan Plateau during 2000–2017 Using Multiple Altimetric Missions and Landsat-Derived Lake Shoreline Positions. *Earth Syst. Sci. Data* **2019**, *11*, 1603–1627. https://doi.org/10.5194/essd-11-1603-2019.
17. Raney, R.K. The Delay/Doppler Radar Altimeter. *IEEE Trans. Geosci. Remote Sens.* **1998**, *36*, 1578–1588. https://doi.org/10.1109/36.718861.
18. Rosen, P.A.; Hensley, S.; Joughin, I.R.; Li, F.K.; Madsen, S.N.; Rodríguez, E.; Goldstein, R.M. Synthetic Aperture Radar Interferometry. *Proc. IEEE* **2000**, *88*, 333–382.
19. Bufton, J.L. Laser Altimetry Measurements from Aircraft and Spacecraft. *Proc. IEEE* **1989**, *77*, 463–477. https://doi.org/10.1109/5.24131.
20. Cretaux, J.-F.; Calmant, S.; Papa, F.; Frappart, F.; Paris, A.; Berge-Nguyen, M. Inland Surface Waters Quantity Monitored from Remote Sensing. *Surv. Geophys.* **2023**, *44*, 1519–1552. https://doi.org/10.1007/s10712-023-09803-x.
21. Durand, M.; Fu, L.-L.; Lettenmaier, D.P.; Alsdorf, D.E.; Rodriguez, E.; Esteban-Fernandez, D. The Surface Water and Ocean Topography Mission: Observing Terrestrial Surface Water and Oceanic Submesoscale Eddies. *Proc. IEEE* **2010**, *98*, 766–779. https://doi.org/10.1109/JPROC.2010.2043031.

22. Davis, C.H. A Surface and Volume Scattering Retracking Algorithm for Ice Sheet Satellite Altimetry. *IEEE Trans. Geosci. Remote Sens.* **1993**, *31*, 811–818. https://doi.org/10.1109/36.239903.
23. Tylmann, W.; Zolitschka, B.; Enters, D.; Ohlendorf, C. Laminated Lake Sediments in Northeast Poland: Distribution, Preconditions for Formation and Potential for Paleoenvironmental Investigation. *J. Paleolimnol.* **2013**, *50*, 487–503. https://doi.org/10.1007/s10933-013-9741-7.
24. Zhang, J.; Ji, D.; Liu, F.; Ning, H. Global Assessment of Lake Surface Morphology and Its Impact on Water Volume Estimation. *Water Resour. Res.* **2025**, *61*, e2024WR039627. https://doi.org/10.1029/2024WR039627.
25. Yao, F.; Livneh, B.; Rajagopalan, B.; Wang, J.; Crétaux, J.-F.; Wada, Y.; Berge-Nguyen, M. Satellites Reveal Widespread Decline in Global Lake Water Storage. *Science* **2023**, *380*, 743–749. https://doi.org/10.1126/science.abo2812.
26. Chaudhary, A.; Agarwal, N.; Sharma, R.; Ojha, S.P.; Kumar, R. Nadir Altimetry Vis-à-Vis Swath Altimetry: A Study in the Context of SWOT Mission for the Bay of Bengal. *Remote Sens. Environ.* **2021**, *252*, 112120. https://doi.org/10.1016/j.rse.2020.112120.
27. Fu, L.-L.; Ubelmann, C. On the Transition from Profile Altimeter to Swath Altimeter for Observing Global Ocean Surface Topography. *J. Atmos. Ocean. Technol.* **2014**, *31*, 560–568. https://doi.org/10.1175/JTECH-D-13-00109.1.
28. Fjørtoft, R.; Gaudin, J.-M.; Pourthié, N.; Lalaurie, J.-C.; Mallet, A.; Nouvel, J.-F.; Martinot-Lagarde, J.; Oriot, H.; Borderies, P.; Ruiz, C. KaRIn on SWOT: Characteristics of near-Nadir Ka-Band Interferometric SAR Imagery. *IEEE Trans. Geosci. Remote Sens.* **2013**, *52*, 2172–2185.
29. Yao, J.; Xu, N.; Wang, M.; Liu, T.; Lu, H.; Cao, Y.; Tang, X.; Mo, F.; Chang, H.; Gong, H.; et al. SWOT Satellite for Global Hydrological Applications: Accuracy Assessment and Insights into Surface Water Dynamics. *Int. J. Digit. Earth* **2025**, *18*, 2472924. https://doi.org/10.1080/17538947.2025.2472924.
30. Parrish, C.; Magruder, L.; Neuenschwander, A.; Forfinski-Sarkozi, N.; Alonzo, M.; Jasinski, M. Validation of ICESat-2 ATLAS Bathymetry and Analysis of ATLAS's Bathymetric Mapping Performance. *Remote Sens.* **2019**, *11*, 1634. https://doi.org/10.3390/rs11141634.
31. Kaya, Y. Evaluation of Icesat-2 Laser Altimetry for Inland Water Level Monitoring: A Case Study of Canadian Lakes. *Water* **2025**, *17*, 1098. https://doi.org/10.3390/w17071098.
32. Zhao, Y.; Fu, J.; Pang, Z.; Jiang, W.; Zhang, P.; Qi, Z. Validation of Inland Water Surface Elevation from SWOT Satellite Products: A Case Study in the Middle and Lower Reaches of the Yangtze River. *Remote Sens.* **2025**, *17*, 1330. https://doi.org/10.3390/rs17081330.
33. Patidar, G.; Indu, J.; Karmakar, S. Performance Assessment of Surface Water and Ocean Topography (SWOT) Mission for WSE Measurement across India. *Geophys. Res. Lett.* **2025**, *52*, e2025GL115804. https://doi.org/10.1029/2025gl115804.
34. Charoensuk, T.; Luchner, J.; Bauer-Gottwein, P. Leveraging Ice, Cloud, and Land Elevation Satellite-2 Laser Altimetry and Surface Water Ocean Topography Radar Altimetry for Error Diagnosis in Hydraulic Models: A Case Study of the Chao Phraya River. *Remote Sens.* **2025**, *17*, 621. https://doi.org/10.3390/rs17040621.
35. Zhou, Y.; Li, Z.; Li, J.; Zhao, R.; Ding, X. Glacier Mass Balance in the Qinghai–Tibet Plateau and Its Surroundings from the Mid-1970s to 2000 Based on Hexagon KH-9 and SRTM DEMs. *Remote Sens. Environ.* **2018**, *210*, 96–112. https://doi.org/10.1016/j.rse.2018.03.020.
36. Zhou, J.; Wang, L.; Zhong, X.; Yao, T.; Qi, J.; Wang, Y.; Xue, Y. Quantifying the Major Drivers for the Expanding Lakes in the Interior Tibetan Plateau. *Sci. Bull.* **2022**, *67*, 474–478. https://doi.org/10.1016/j.scib.2021.11.010.
37. Zhang, G.; Luo, W.; Chen, W.; Zheng, G. A Robust but Variable Lake Expansion on the Tibetan Plateau. *Sci. Bull.* **2019**, *64*, 1306–1309. https://doi.org/10.1016/j.scib.2019.07.018.
38. Neeck, S.P.; Lindstrom, E.J.; Vaze, P.V.; Fu, L.-L. Surface Water and Ocean Topography (SWOT) Mission. In *Proceedings of the Sensors, Systems and Next-Generation Satellites XVI, Edinburgh, United Kingdom, 24–27 September 2012*; Meynart, R., Neeck, S.P., Shimoda, H., Eds.; SPIE: Bellingham, WA, USA, 2012; p. 85330G.
39. Biancamaria, S.; Lettenmaier, D.P.; Pavelsky, T.M. The SWOT Mission and Its Capabilities for Land Hydrology. *Surv. Geophys.* **2016**, *37*, 307–337. https://doi.org/10.1007/s10712-015-9346-y.

40. Li, D.; Andreadis, K.M.; Margulis, S.A.; Lettenmaier, D.P. A Data Assimilation Framework for Generating Space-Time Continuous Daily SWOT River Discharge Data Products. *Water Resour. Res.* **2020**, *56*, e2019WR026999. https://doi.org/10.1029/2019WR026999.
41. Zhang, G.; Xie, H.; Kang, S.; Yi, D.; Ackley, S.F. Monitoring Lake Level Changes on the Tibetan Plateau Using ICESat Altimetry Data (2003–2009). *Remote Sens. Environ.* **2011**, *115*, 1733–1742. https://doi.org/10.1016/j.rse.2011.03.005.

Disclaimer/Publisher's Note: The statements, opinions and data contained in all publications are solely those of the individual author(s) and contributor(s) and not of MDPI and/or the editor(s). MDPI and/or the editor(s) disclaim responsibility for any injury to people or property resulting from any ideas, methods, instructions or products referred to in the content.